Investigation of the Aerodynamics Performance of Horizontal Axis Wind Turbine Rotor

Daramola Oyewole Olufemi

Abstract – In order to convert wind energy to mechanical energy, the design of the axis wind turbine is very crucial, the rotor is an important component of the wind turbine. This study investigates the aerodynamics performance of horizontal axis wind turbine rotor. By obtaining the power coefficient, we found that about forty percent of the kinetic energy of the undisturbed wind flowing to the swept area of the rotor can be extracted as useful power. Also, we found that the twisting of the blades of a horizontal axis wind turbine has a positive impact on the performance of its rotor, as twisting optimize angle of attack and maximize the lift force. Other factors such as high lift-to-drag ratio, high maximum lift coefficient and high tip speed ratio were found to bring about improvement to the performance of a horizontal axis wind turbine.

Index Terms – Wind turbine, aerodynamics, horizontal wind turbine, turbine blade

1 INTRODUCTION

Wind energy has risen to become one of the most applied form of renewable energy [1]–[5]. Different processes and plants utilizes wind energy [6]–[17]. Horizontal axis wind turbine is the most commercially available and has gained the attention of investors [18].

The aerodynamic performance of an Horizontal Axis wind turbine rotor depends largely on design parameters including number of blades, airfoil shapes, blade twist along the rotor radius, blade pitch, tip speed ratio and rotor hub height (or tower height) [19]:

In addition, the aerodynamic performance of a Horizontal Axis Wind Turbine rotor can be evaluated using: Blade Element Theory and Momentum Theory [19]. The blade element theory assumes that each blade of a horizontal axis wind turbine can be divided into many small “elements” that are independent of other elements and operates aerodynamically as 2D air-foils [19]. Also, the blade theory is based on two main assumptions: No aerodynamic interactions exist between the different blade elements and the lift and drag coefficients solely determine the forces on the blade elements [20].

On the other hand, the momentum theory considers momentum loss through the plane of the rotor based on work done by the wind [19]. The combination of “blade element” and “momentum” theories give arise to the Blade Element Momentum (BEM) theory [19]. The “BEM” theory is used to determine the total thrust and thrust on a horizontal axis wind turbine blade through an iterative process- which is carried out for each blade element [19]. The iterative process for each blade element is as follows:

1. Initialize the tangential induction factor, a', to be zero and the axial induction factor, a, to be any value.
2. Determine the inflow angle, ∅, using:
$$\emptyset = \tan^{-1}\left[\frac{U_\infty(1-a)}{\Omega r(1+a')}\right]$$
3. Determine the angle of attack ”a” for the airfoil: α=$\emptyset - \beta$.
4. Check for the drag and lift coefficient, $C_D$and $C_L$from the performance dataset gotten from XFOIL or XFLR5 program.
5. Determine the thrust and torque contribution from the annulus using Blade Element Theory:

   Total thrust “dT” for “B” number of blades is given as:

   $$dT=\frac{B}{2}\rho V^2{}_{total}[C_L\cos\emptyset+C_D\sin\emptyset]cdr.$$

   Also, the total torque “dQ” for “B” number of blades is given as:

   $$dQ=\frac{B}{2}\rho V^2{}_{total}[C_L\sin\emptyset-C_D\cos\emptyset]crdr.$$
6. Update the values of axial induction factor “a” and tangential induction

   factor "a'", using the momentum theory. The following equations are used to update the values of the two induction factors:

   Thrust extracted by each rotor annulus, dT= $4\pi r\rho U_\infty{}^2$(1-a) adr

   Torque extracted by each rotor annulus, dQ= $4\pi r^3\rho U_\infty\Omega$ (1-a) a'dr.
7. Repeat the above procedures from step 2 to step 6 until the values of “a” and "a'" converge.
8. The above calculation is done for each element. Thus, we can sum up the thrust and torque of all the elements to obtain the rotor thrust and torque. Finally, the power

- *Daramola Oyewole Olufemi is currently affiliated to the National Metallurgical Development Centre, Jos, Nigeria. Email: darafemmie11@gmail.com*

generated by the rotor and its power coefficient are calculated.

1.1 Estimation of Reynold's Number and The Local Total Velocity

The given parameters in the question include:

Rotor radius 'R'=6m,

Diameter of Rotor 'D'=2R=2×6=12m

Length of blade, L=5m

Airfoil adopted = "NACA 0020"

Chord Length 'c'=1m

Angular velocity of rotor 'Ω'=6rad/s

Natural wind speed '$U_\infty{}'$=8m/s

Density of air 'ρ'=1.2kg/m^3

Viscosity of air 'μ'=1.8×$10^{-5} kgm^{-1}s^{-1}$

a. To calculate local total velocity at mid-span of the blade "V_{total} ", the diagram below is considered:

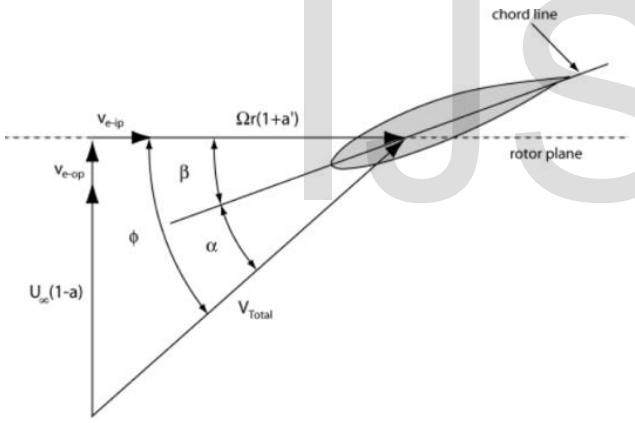

Figure 1: Vector representation of the velocity components of a wind turbine blade [19]**.**

From Pythagoras' theorem:

$$V^2{}_{total}=[\Omega r(1+a')]^2 + [U_\infty(1+a)]^2$$

Where axial induction factor "a" and tangential induction factor "a'" equal to zero

Thus, V_{total} becomes:

$V^2{}_{total}=(\Omega r)^2+U_\infty{}^2$ where r=3.5m (i.e. radius at mid-span of the blade)

Recall, Linear velocity of rotor rotation at mid-span v= Ωr=6× 3.5 =21m/s

$$V^2{}_{total}=21^2 + 8^2= 441+64= 505$$

$$V_{total}=\sqrt{505}=22.5\text{m/s}\approx 23\text{m/s}$$

Therefore, the total local velocity at mid-span of the blade, V_{total} is 23m/s.

Representative Reynold's number for the rotating blades 'Re':

$$\text{Re}=\frac{Density\ of\ air\times \text{Total local velocity}\times \text{Charasteristic length}}{Viscosity\ of\ air}=\frac{\rho\times V_{total}\times c}{\mu}$$

Where characteristic length = chord length='c'

$$\text{Re}=\frac{1.2\times 23\times 1}{1.8\times 10^{-5}}=1{,}533{,}333= 1.5\times 10^6$$

Therefore, the Reynold's number for the rotating blades is 1.5× 10^6 .

1.2 Aerodynamic Coefficients and X-foil Program Execution

1.2.1. Definition of Aerodynamic Coefficients

The definitions of lift and drag coefficients are as shown below:

Lift coefficient is a dimensionless parameter that shows the relationship between the lift force 'F_L' acting on a 2D airfoil, density of air 'ρ', wind speed 'U' and reference area 'A'.

$$\text{Lift Coefficient, } C_L=\frac{F_L}{\frac{1}{2}\rho U^2 A}$$

Drag coefficient is a dimensionless parameter that indicates the relationship between the drag force 'F_D' acting on a 2D airfoil, density of air 'ρ', wind speed 'U' and reference area 'A'.

$$\text{Drag Coefficient, } C_D=\frac{F_D}{\frac{1}{2}\rho U^2 A}$$

where 'F_L' is the lift force (in Newton), 'F_D' is the drag force (in Newton), ρ is the density of air (in Kg/m^3), 'A' is the reference area and 'U' is the upstream wind velocity.

1.2.2. X-Foil Program Execution and Results

The following parameters were used in the X-FOIL program to get the relationship between various parameters:
Reynold's Number Re=1,500,000
Range of angles of attack: $0^\circ < \alpha < 30^\circ$ (i.e.'α' lies between 1 and 29, with both numbers inclusive)
Angle of attack increment, $\Delta\alpha = 1^\circ$ NACA 0020 was adopted
The table below shows the values of lift coefficient '$C_L{}'$, drag coefficient 'C_D' and angle of attack 'α' exported from the X-foil program:

Table 1: Variation of angle of attack 'α' with lift coefficient 'C_L'and drag coefficient 'C_D'.

Angle of Attack, α	Lift Coefficients, C_L	Drag Coefficient, C_D
1	0.1103	0.00722
2	0.2202	0.00731
3	0.3292	0.0075
4	0.437	0.0078
5	0.5436	0.00817
6	0.6481	0.00868
7	0.7499	0.00933
8	0.8477	0.01012
9	0.9383	0.01106
10	1.0233	0.01224
11	1.1403	0.01382
12	1.2562	0.01567
13	1.2814	0.01731
14	1.338	0.01992
15	1.3908	0.02351
16	1.4345	0.02834
17	1.4633	0.03509
18	1.4827	0.04354
19	1.4812	0.05488
20	1.4624	0.06895
21	1.4132	0.08756
22	1.3743	0.1056
23	1.3179	0.012688
24	1.2775	0.14661
25	1.2551	0.16422
26	1.2319	0.18241
27	1.2283	0.19762
28	1.2231	0.2133
29	1.2265	0.22707

The graphs below show the variation of angle of attack 'α' with lift coefficient 'C_L' and drag coefficient 'C_D' :

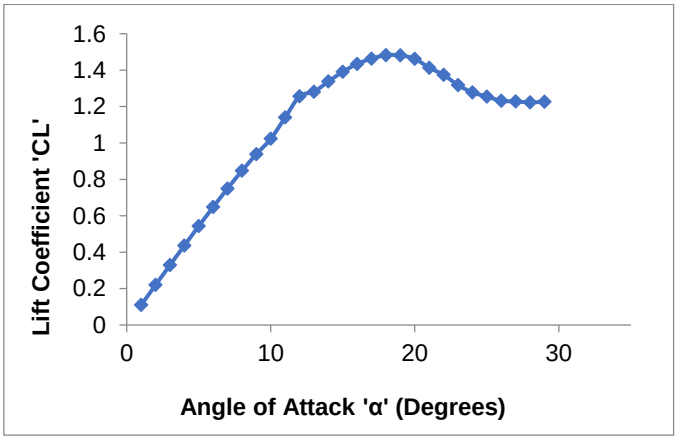

Figure 2 Variation of lift coefficient with respect to angle of attack

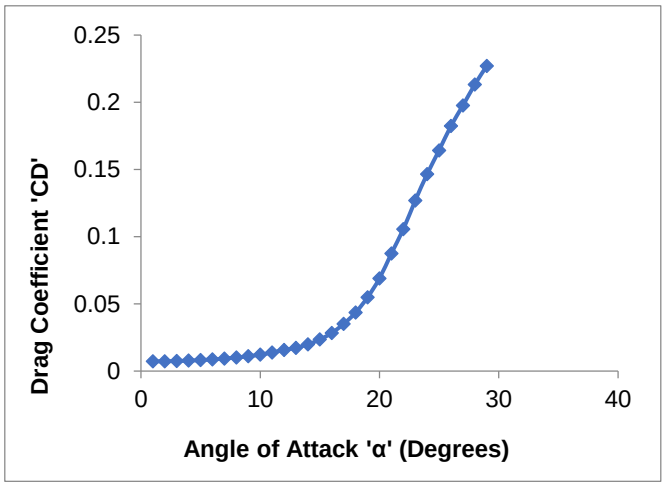

Figure 3 Variation of drag coefficient with respect to angle of attack

1.3 Blade Element Momentum Theory

Pitch angle 'β'=8°,

Tangential induction factor a'= 0

Lift coefficient 'C_L'=1.25 Drag coefficient 'C_D'= 0.24+0.015(α-30)

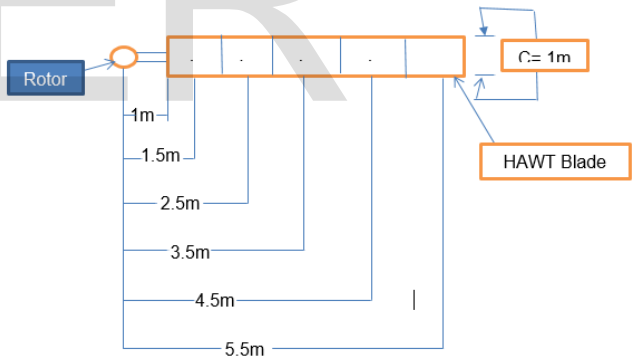

Figure 4 Distance of blade elements from the rotor centre.

From the figure above, the blade is divided into five elements. Also, It is clearly seen from the figure that r_1=1.5m, r_2=2.5m, r_3=3.5m, r_4=4.5m and r_5=5.5m. These values were used in the iteration process discussed in section 3.1. using BEM theory and a MATLAB code was written to perform the iteration process. This MATLAB code can be viewed in the appendix section of this report.

The total thrust and torque obtained from the iteration code written using MATLAB are:

Total Thrust 'T' = 2.2750 × 10^3 N

Total Torque 'Q' = 2.3191× 10^3Nm.

The power generated 'P_G' by the rotor is given by:

Power generated 'P_G' = Total Torque 'Q' × angular velocity of the rotor 'Ω'

Power generated, 'P_G' = 2.3191× $10^3 N/m$ ×6rad/s=13914.6Watts

To calculate the power coefficient, $'C_P' = \frac{Power\ Generated}{Power\ Available} = \frac{P_G}{\frac{1}{2}\rho A U_\infty{}^3}$

Where A = Cross Sectional Area,

A = $\pi R^2 = \pi \times 6^2$= 36πm^2=113.1m^2

Power Coefficient $'C_P' = \frac{13914.6}{\frac{1}{2}\times 1.2\times 113.1\times 8^3} = \frac{13914.6}{34744.3}$ = 0.40

The value of $'C_P'$ obtained above indicates that about forty percent of the kinetic energy of the undisturbed wind is extracted as useful power.

1.4 Effect of Blade Twist on Rotor Performance

Twisting of a rotor blade affects the angle of attack 'α' and the lift to drag ratio '$\frac{F_L}{F_D}$' [5]. Continuous twist of blade along its length helps to achieve optimum angle of attack across the blade's cross-section. As a result of this, the lift is maximized (i.e. high lift to drag ratio is obtained), thus increasing rotational moment and the power output of the turbine rotor [5], [13].

2 ESTIMATION OF THE TOTAL VERTICAL FORCE ACTING ON A PLATFORM DUE TO THE DYNAMIC FORCE ONLY

The following parameters were given to solve the questions in this chapter**:**

Diameter of each of the two submerged cylinders 'D' = 10m.

Draft 'T' = 20m,

Width of submersible platform 'L'= 54m

Seawater density 'ρ'= 1025kg/m^3, Gravitational acceleration 'g'=9.81m/s^2

Monochromatic wave frequency 'ω_w'= 0.6rad/s

Wave height 'H_w' = 7m.

In addition, deep water condition is assumed to be valid.

From Airy wave theory, the velocity potential expression is given by:

ϕ = −a$\frac{\omega}{K} e^{ky} cos\ (kx - \omega t)$ for deep water condition

Recall dynamic pressure 'P_d' is given by:

$P_d(x,y,t)$ = - ρ$\frac{\partial \emptyset(x,y,t)}{\partial t}$

Differentiating the expression for 'ϕ' partially with respect to 't', we have:

$\frac{\partial \emptyset(x,y,t)}{\partial t} = \frac{\partial}{\partial t}[-a\frac{\omega}{K} e^{ky} cos\ (kx - \omega t)]$

$\frac{\partial \emptyset(x,y,t)}{\partial t}$ = -a$\frac{\omega}{k} e^{ky} \times -\omega \times -\sin(kx - \omega t)$

$\frac{\partial \emptyset(x,y,t)}{\partial t}$ = -a$\frac{\omega^2}{k} e^{ky} \sin(kx - \omega t)$

Therefore, the dynamic pressure is given by the expression:

$P_d(x,y,t)$= - ρ[-a$\frac{\omega^2}{k} e^{ky} \sin(kx - \omega t)$]

$Dynamic\ Pressure, P_d(x,y,t) = \rho a\frac{\omega^2}{k} e^{ky} \sin(kx - \omega t)$

In order to get the final expression for the dynamic pressure, the unknown parameters in the above expression need to be found as shown below:

Amplitude 'a' =$\frac{H_w}{2} = \frac{7}{2}$ = 3.5m,

Wave Period 'T_w' = $\frac{2\pi}{\omega_w} = \frac{2\pi}{0.6}$ = 10.47s

Wavelength 'λ' = 1.56× $T_w{}^2$ = 1.56× 10.47^2 = 171m

Wave number 'k' = $\frac{2\pi}{\lambda} = \frac{2\times 3.142}{171}$ = 0.037rad/m

The final expression for the dynamic pressure is:

$P_d(x,y,t) = 1025\times 10.47\times \frac{0.6^2}{0.037} \times e^{0.037y} \times \sin(0.037x - 0.6t)$

$P_d(x,y,t) = 104417e^{0.037y} \sin(0.037x - 0.6t) N/m^2.$

2.1 Heave Equation of Motion

The heave equation of motion (time domain), assuming that at first approximation the heave degree of freedom is decoupled from the other degree of freedom is given by:

(m + A) z'' + Cz = F(t)

Where m= mass of the submersible, A= added mass

C= hydrostatic stiffness.

Since the body is a freely floating body, Archimedes' principle can be applied:

Weight of fluid displaced = Weight of the floating body

ρVg=mg. Therefore, mass of the body 'm' can be obtained from:

Mass of floating body= ρ× V

where displaced volume 'V' =submerged volume=$2\pi r^2 T$

Displaced volume 'V' = $2\times \pi \times 5^2 \times 20 = 3141.6m^3$

Mass of floating body 'm' = $1025 \times 3141.6 = 3220140kg/m^3 = 3.22\times 10^6 kg/m^3$

The added mass coefficient ''C_a' chosen from the appendix of [21]DNV RP (2014) by considering the vertical motion of the body and its body shape (chosen as circular disc) is:

Added mass coefficient 'C_a' = $(\frac{2}{\pi})$ = 0.64

To calculate the restoring coefficient 'C' , we have:

Restoring coefficient 'C' = $2\pi\rho g r^2 = 2\times \pi \times 1025 \times 9.81 \times 5^2 =$ 1579475N/m

The heave undampened natural frequency of the submersible can be estimated as shown below:

Undampened natural frequency 'ω_0'= $\sqrt{\frac{C}{m+A}}$

Undampened natural frequency 'ω_0' = $\sqrt{\frac{1579475}{3220140+A}}$

Where added mass 'A' $=2 \times C_a \times \rho \times V_R = 2 \times 0.64 \times 1025 \times \frac{4}{3}\pi \times 5^3$

(Reference Volume $=\frac{4}{3}\pi R^3$)

Added mass 'A' = 687050.7kg
Thus, Undampened natural frequency becomes:

Undampened natural frequency,

$$'\omega_0' = \sqrt{\frac{1579475}{3220140+687050.7}} = \sqrt{\frac{1579475}{3907190.7}}$$

$'\omega_0'$ = 0.64rad/s.

2.2 Natural Frequency in Heave Versus Typical Wave Energy Spectra

The following parameters were substituted into the Pierson-Moskowitz $S_{PM}(\omega)$ and JONSWAP wave spectrum $S_j(\omega)$ with the value of frequency 'ω' from 0 to 4.0: γ=3.3, H=7m, ω_p =0.6rad/s, σ= 0.09 (since ω> ω_p),

A=1-ln γ=1-ln(3.3) = 0.657344252.

The varied values of $'\omega'$ are plotted against the corresponding values of PM spectrum and JONSWAP spectrum. The natural frequency in heave 'ω_0' of the platform coincides with the highest energy spectrum for both Pierson-Moskowitz $S_{PM}(\omega)$ and JONSWAP wave spectrum $S_j(\omega)$. Also, it is clearly seen from the graph below that JONSWAP wave spectrum $S_j(\omega)$ has more energy than Pierson-Moskowitz $S_{PM}(\omega)$ wave spectrum at the natural frequency (i.e. ω_0 = 0.64rad/s) in heave of the platform obtained from the previous section.

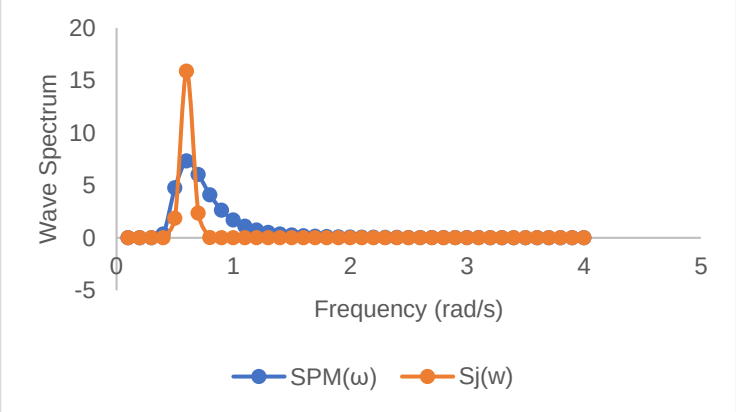

Figure 5 Wave Energy Spectra

3 ESTIMATION OF HIGHEST SIGNIFICANT WAVE HEIGHT USING WEIBULL PDF.

Given parameters include:
Weibull fitting parameter a'=0.5
Added mass coefficient 'C_a' = 1.0
Drag Coefficient 'C_d' = 0.8
Gravitational acceleration 'g' = 9.8m/s^2
Highest wave period 'T_{Hmax}'= 13s
Diameter 'D' = 3m
Length of member 'L' = 15m
Draft 'F' = 75
Return period 'R' =1 year
Seawater density 'ρ' = 1025kg/m^3
Seawater Viscosity 'v'=1.05× $10^{-6}m^2/s$
Water depth 'd' =200m
JONSWAP, peak frequency 'ω_p' = 0.45rad/s
JONSWAP, peak shape par 'γ' = 3.3

Table 2 Weibull Distribution Data

H/m	P_{CL}(H)	$\ln(H-0.5)$	$\ln[\ln(\frac{1}{1-P_{CL}(H)})]$
1	0.074	-0.693	-2.565
2	0.336	0.405	-0.893
3	0.629	0.916	-0.008
4	0.825	1.253	0.556
5	0.925	1.504	0.952
6	0.968	1.705	1.236

7	0.986	1.872	1.451
8	0.994	2.015	1.632
9	0.998	2.140	1.827
10	10	2.251	0

The probability that the wave will be lower than the 1year return wave: P_1(H) =P(H<H_1)= 1-$\frac{3h}{24\frac{h}{d}\times 365.25\frac{d}{y}\times 1y} \approx 0.9997$

Thus;

$\ln[\ln(\frac{1}{1-P_1(H)})]=\ln[\ln(\frac{1}{1-0.9997})]=2.093$

With the table above, a Weibull plot was created as shown below:

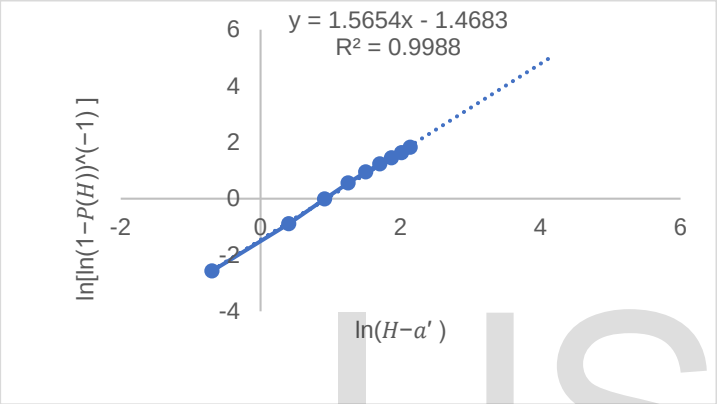

Figure 6 Weibull Plot

It can be seen from the Weibull plot that the equation of the line is:

Y=1.5654x-1.4683 and

Correlation Coefficient "R" =0.9988.

The value of 'R' shows that a very strong relationship exists between the values plotted, as it is close to 1.0. To know the corresponding value of $\ln(1-a')$ (i.e. value on x-axis) when $\ln[\ln(1-P(H))^{-1}]$=2.093, we use the equation of the line described above:

2.093 =1.5654x-1.4683

1.5654x=2.093+1.4683

1.5654x=3.5613.

Thus, x=$\frac{3.5613}{1.5654}$=2.275

Therefore, the corresponding value of $\ln(1-a')$ when $\ln[\ln(1-P(H))^{-1}]$=2.093 is 2.275. Thus, the maximum significant wave height for the 1year return period is given by:

$\ln(H_1-a')$=2.275

$H_1=e^{2.275}$+ a'=9.73+0.5 (where a'=0.5)

H_1=10.23m≈ $10m$

Therefore, the maximum significant wave height for one year return period is 10m.

3.1 Calculation of Highest Wave Height likely to occur in One Year Return Period.

The parameters given to calculate the highest wave height likely to occur are:

JONSWAP, peak frequency 'ω_P' =0.45rad/s

JONSWAP, peak shape par 'γ' = 3.3

Peak frequency 'ω_P'=$\frac{2\pi}{JONSWAP,Peak\ period} = \frac{2\pi}{T_p}$

Thus, JONSWAP, peak period 'T_p' =$\frac{2\pi}{\omega_P}$= $\frac{2\pi}{0.45}$=$\frac{2\times 3.142}{0.45}$= $\frac{6.284}{0.45}$= 13.96s

In section 3.5.5 of DNV-RP-C205[21] , JONSWAP, peak period 'T_p' is approximated as:

T_p=1.2859T_Z, when 'γ' = 3.3

T_Z=$\frac{T_p}{1.2859} = \frac{13.96}{1.2859}$ = 10.86s

Thus, the zero up-crossing wave period, T_Z is 10.86s.

Thus, to calculate the mean wave period T_1=1.0734T_Z= 1.0734×10.86

Mean wave period T_1 = 11.66s.

Therefore, the total number of waves 'N_{waves}' to be encountered in 3 hours is given by:

N_{waves}= $\frac{t}{T_1} = \frac{3\times 3600}{11.66}$ = 926.24waves

N_{waves} ≈ 926 waves will be encountered

The probability of obtaining the highest wave likely to occur is:

P (H_{max}) = $\frac{N_{waves}-1}{N_{waves}} = \frac{926-1}{926}$

P (H_{max}) = $\frac{925}{926}$ = 0.999

The highest wave likely to occur in the given return period, H_{max} is given by:

H_{max}=$\sqrt{\ln(1-P(H_{max}))} \times \frac{H^2{}_{1/3}}{-2}$ where $H_{1/3} = 10.23m$

H_{max}= $\sqrt{\ln(1-0.999)} \times \frac{10.23^2}{-2}$

H_{max}=$\sqrt{361.458}$ = 19.01m≈19m.

Therefore, the highest wave likely to occur in the given return period is 19m.

3.2 Selection of Appropriate Wave Theory

In order to select the appropriate wave theory, we need to calculate the following parameters:

1. $\frac{d}{\lambda}$: To calculate the wavelength 'λ' of the wave we use:

λ = 1.56× $T^2{}_{Hmax}$ where T_{Hmax}= 13s.

λ =1.56 X13^2= 1.56 X169

λ=263.64m.

Given depth of water 'd'=200m: $\frac{d}{\lambda}$= $\frac{200}{263.64} \approx 0.76$

Since $\frac{d}{\lambda} \gg \frac{1}{20}$ (i.e. 0.76≫0.05), therefore we assume deep-water condition.

2. $\frac{H}{gT^2}$: To calculate this, we use the values of H_{max} and T_{Hmax} as stated in the question:

$$\frac{H_{max}}{gT^2_{Hmax}} = \frac{19}{9.81\times13^2} = \frac{19}{9.81\times169} = \frac{19}{1657.89} = 0.0115.$$

Where acceleration due to gravity 'g' =9.81m/s^2

3. $\frac{d}{gT^2}$: To calculate this, we use the values of 'd' and T_{Hmax} as stated in the question:

$$\frac{d}{gT^2_{Hmax}} = \frac{200}{9.81\times13^2} = \frac{200}{9.81\times169} = \frac{200}{1657.89} = 0.121.$$

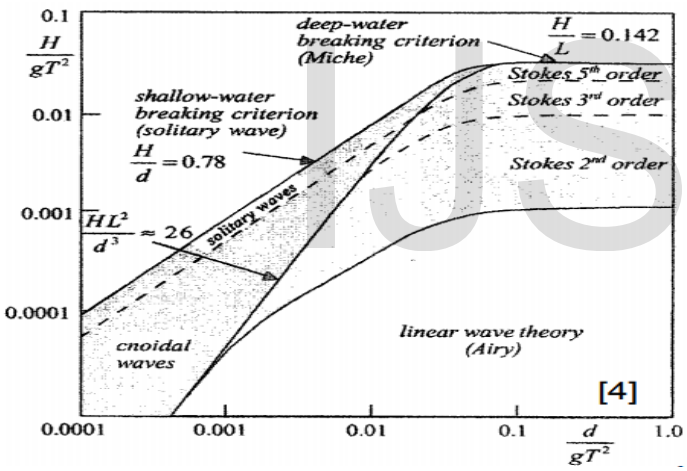

Figure 7 Graph of range of validity for wave theories [22]**.**

From the figure above, by tracing the point 0.0115 on the vertical axis and 0.121 on the horizontal axis, it is seen that the point of intersection of these two points in the Stoke's 3^{rd} order region of the graph. Thus, Stoke's 3^{rd} order should be used.

3.3 Estimation of Wave Force Using Morison Approach

In order to demonstrate that the wave force can be estimated using Morison approach [23], [24], we need to calculate the parameters listed below:

1. $\frac{Member\ Diameter}{Wavelength} = \frac{D}{\lambda}$:

If $\frac{D}{\lambda} < 0.2$, then the characteristics of the incident wave is not significantly altered (i.e. a small volume structure), therefore Morison equation will be applicable.Thus: Where Member Diameter 'D' = 3m

Wavelength 'λ'= 263.64m (as calculated in section 3.3)

Therefore; $\frac{D}{\lambda}$=$\frac{3}{263.64}$ = 0.0114

Since 0.0114≪ 0.2, Morison equation is applicable to estimate the wave force.

2. Keulegan-Carpenter number $'K_C' = \frac{U_m \times T_{Hmax}}{D}$

Where U_m= Maximum normal water particle velocity, D= Member Diameter = 3m, T_{Hmax}= Highest wave Period= 13s.

The value of $'U_m'$ can be determined from Airy wave theory velocity potential as shown below:

$$\phi = -a\frac{\omega}{K} e^{ky} cos\ (kx - \omega t)$$

The above equation holds for deep water condition.

The vertical velocity is given by:

$$U = \frac{\partial\phi}{\partial X} = \frac{\partial}{\partial X}\left[-a\frac{\omega}{K}e^{ky}\cos(kx - \omega t)\right]$$

$$U = a\omega e^{ky}\sin(kx - wt)$$

Therefore, the maximum horizontal velocity $'U_m'$ occurs at waterline level (i.e. y=0) and when $(kx - wt)$ equals 90°, thus:

$$U_m = a\omega = \frac{H_{max}}{2} \times \frac{2\pi}{T_{Hmax}} = \frac{\pi H_{max}}{T_{Hmax}}$$

$$U_m = \frac{3.142\times19}{13} = 4.59 m/s.$$

Now, the Keulegan-Carpenter number $'K_C'$ can be estimated as:

$$K_c = \frac{4.59\times13}{3} = 19.89$$

Since 5< K_c <25 (i.e. 5< 19.89 <25), only Morison equation is applicable to estimate the wave force. The table below explains this better, as this situation falls in the intermediate regime based on the values obtained above:

	D/λ < 0.20	D/λ > 0.20
K-C > 25 (H/D > 8) (Deepwater K-C~πH/D)	**DRAG DOMINATED** *Morison Eqn.* C_M = 1.8 C_D function of *Re*	(no waves here, above breaking condition)
5 < K-C < 25 (1.5 < H/D < 8)	**INTERMEDIATE REGIME** Complex flow, exp data wide scatter *Morison Eqn* For Re > 1.5E06 C_M = 1.8 C_D = 0.62	(no waves here, above breaking condition)
K-C < 5 (H/D < 1.5)	**INERTIA DOMINATED** *Morison Eqn / Diffraction Theory* C_M = 2.0 C_D = negligible	*NO Morison Eqn* *Diffraction Theory*

Figure 8 Wave Loading Regimes [25]**.**

To derive the expression for the total vertical force due to the wave acting on the offshore structure [26]–[30] (i.e. a horizontal cylinder normal to the wave), we have:

Total Vertical Force F_V = Inertia Force (F_I) + Drag force (F_D)

$$F_V = \int_{\frac{-L}{2}}^{\frac{L}{2}} (C_M \rho \pi r^2 \dot{V} dx + C_D \rho r|V|Vdx)$$

Where C_M= Inertia Coefficient=added mass coefficient + 1= $C_a + 1$

Given added mass coefficient $C_a = 1$; Thus C_M= 1+1= 2

Seawater density 'ρ' = 1025kg/m^3, Radius 'r' =$\frac{D}{2} = \frac{3}{2}$ =1.5m

Length 'L' =15m Drag coefficient 'C_D'= 0.8

The values of vertical acceleration '$\dot{V}$' and vertical velocity 'V' can be calculated using Airy wave theory velocity potential as shown below:

$\phi = -a\frac{\omega}{K} e^{ky} cos\,(kx - \omega t)$ for deep water condition

Vertical velocity 'V' = $\frac{\partial \phi}{\partial Y} = \frac{\partial}{\partial Y}\left[-a\frac{\omega}{K} e^{ky} \cos(kx - \omega t)\right]$

Vertical velocity 'V'= -a$\omega e^{ky} \cos(kx - \omega t)$

Vertical acceleration '$\dot{V}$' =$\frac{\partial V}{\partial t} = \frac{\partial}{\partial t}$[-a$\omega e^{ky} \cos(kx - \omega t)$]

Vertical acceleration '$\dot{V}$'= -a$\omega^2 e^{ky} \sin(kx - \omega t)$

The values of wave number 'k', amplitude 'a' and circular frequency 'ω' are calculated as shown below:

Wave number 'k' =$\frac{2\pi}{\lambda} = \frac{2\times3.142}{263.64} = \frac{6.284}{263.64} \approx$ 0.024rad/m,

Amplitude 'a' = $\frac{H_{max}}{2} = \frac{19}{2}$ = 9.5m,

Circular Frequency 'ω' = $\frac{2\pi}{T_{Hmax}} = \frac{2\times3.142}{13} = \frac{6.284}{13} \approx$0.48rad/s.

Therefore, the expressions for the vertical velocity 'V' and vertical acceleration '$\dot{V}$' are shown below:

Vertical velocity 'V' = -9.5×0.48× $e^{0.024y} \times \cos(0.024x - 0.48t)$

'V'= -4.56$e^{0.024y} \cos(0.024x - 0.48t)$

Vertical acceleration '$\dot{V}$'= -9.5× $0.48^2 \times e^{0.024y} \times \sin(0.024x - 0.48t)$

'$\dot{V}$' = -2.189$e^{0.024y} \sin(0.024x - 0.48t)$

The total vertical force becomes:

Total vertical force F_V= $\int_{\frac{-15}{2}}^{\frac{15}{2}} (C_M \rho \pi r^2 \dot{V} dx + C_D \rho r|V|Vdx)$

Vertical Inertia force F_I= $\int_{-7.5}^{7.5} C_M \rho \pi r^2 \dot{V} dx$

F_I= $\int_{-7.5}^{7.5}$ [$2 \times 1025 \times 3.142 \times 1.5^2 \times -2.189e^{0.024y} \sin(0.024x - 0.48t)$ dx]

$F_I = \int_{-7.5}^{7.5}$ [-31724.03$e^{0.024y} \sin(0.024x - 0.48t)$ dx]

F_I = -31724.03$e^{0.024y} \int_{-7.5}^{7.5}$ [$\sin(0.024x - 0.48t)$ dx]

F_I =31724.03$e^{0.024y}$[$\frac{\cos(0.024x-0.48t)}{0.024}$]$_{-7.5}^{7.5}$= $\frac{31724.03}{0.024} e^{0.024y}[\cos(0.024x - 0.48t)]_{-7.5}^{7.5}$

F_I =1321834.6$e^{0.024y}$[cos((0.024 × 7.5) − 0.48t) - cos((0.024 × −7.5) − 0.48t)]

F_I =1321834.6$e^{0.024y}$[cos(0.18 − 0.48t) - cos(−0.18 − 0.48t)]

F_I= 1321834.6 $e^{0.024y}$ [cos(0.18 − 0.48t) − cos(−0.18 − 0.48t)]

Taking y=0

$F_I = 1321834.6[\cos(0.18 - 0.48t) - \cos(-0.18 - 0.48t)]$

Therefore, the inertia force component 'F_I' of the vertical force is $1321834.6[\cos(0.18 - 0.48t) - \cos(-0.18 - 0.48t)]$.

To calculate the Drag force component, F_D, of the total vertical force, we have:

$$F_D = \int_{-7.5}^{7.5} C_D \rho r |V| V dx$$

$$F_D = \int_{-7.5}^{7.5} [0.8 \times 1025 \times 1.5 \times |-4.56e^{0.024y}\cos(0.024x - 0.48t)| \times (-4.56e^{0.024y}\cos(0.024x - 0.48t))]dx$$

$$F_D = 25576.13 \int_{-7.5}^{7.5} [|e^{0.024y}\cos(0.024x - 0.48t)| \times (e^{0.024y}\cos(0.024x - 0.48t))]dx$$

Taking y=0, the above integral for drag force component 'F_D' is evaluated using MATLAB software and the result is shown below:

F_D =532836.04sin(0.096t) -266418sin(0.096t − 0.36) - 266418sin(0.096t + 0.36)

The total vertical force acting on the offshore structure is:

$$F_V = F_I + F_D$$

Th e total vertical force acting on the offshore structure is:

$$F_V = 1321834.6e^{0.024y}[\cos(0.18 - 0.48t) - \cos(-0.18 - 0.48t)] + 532836.04\sin(0.096t) - 266418\sin(0.096t - 0.36) - 266418\sin(0.096t + 0.36)$$

The figure below shows how inertia force 'F_I' , drag force 'F_D' and total vertical force 'F_V' vary with time:

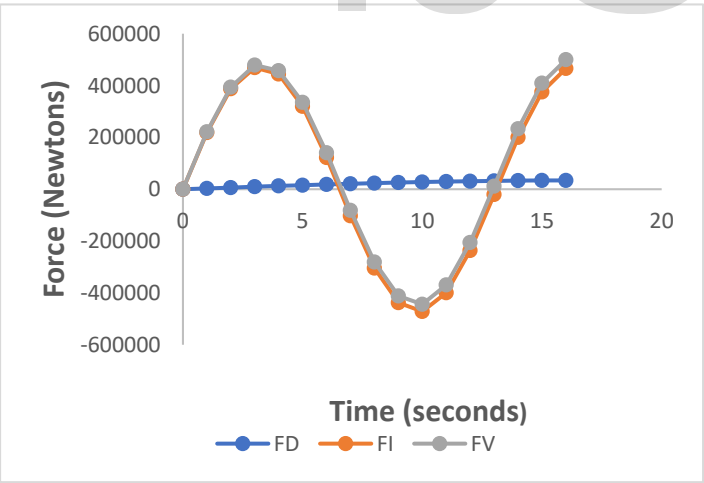

Figure 9 Variation of Force with Time

3.4 Limitations of Approaches Adopted in Previous Steps

Weibull distribution was the approach used in section 3.1 and it can only be used to estimate long-term wave properties, usually 10 years and above[22]. It is obvious that there are no data measurements covering a period of at least 100 years properties, thus estimates rely on extrapolation of wave properties measured by devices over a period of 3 years[22]. In conclusion, Weibull distribution is prone to error as every estimate depends on extrapolation[22].

JONSWAP wave spectrum was used in section 3.2 can only be used to analyze the wave properties of young seas [22]. Also, JONSWAP spectrum is applicable to only random unidirectional sea. Stoke's 3^{rd} order theory suggested in section 3.3 is only applicable for deep water but it isn't applicable for shallow water, when d< $\frac{\lambda}{8}$ [31].

Finally, Morison approach used in section 3.4 is not applicable for calculating the wave loads on an offshore structure when the ratio of its diameter (D) to the wavelength (λ) of the incident wave is greater than 0.2(i.e. $\frac{D}{\lambda} > 0.2$) or when the offshore structure is big enough to change the incident wave characteristics [25].

In addition, the partly used Airy linear wave theory in section 3.4 is not applicable for high height waves, that is why it is referred to as small amplitude theory [22][8], [32].

4 CONCLUSION

The value of the power coefficient (C_p =0.40) obtained in section one indicates that about forty percent of the kinetic energy of the undisturbed wind that flows to the swept area of the rotor can be extracted as useful power [19]. In addition, the twisting of the blades of a horizontal axis wind turbine has a positive impact on the performance of its rotor, as twisting optimize angle of attack and maximize the lift force [19]. Others factors that improves the performance of a horizontal axis wind turbine are high lift-to-drag ratio, high maximum lift coefficient and high tip speed ratio [19], [33]–[35].

More so, the natural frequency in heave 'ω_0' of the platform in section 2 coincides with the highest energy spectrum for both Pierson-Moskowitz $S_{PM}(\omega)$ and JONSWAP wave spectrum $S_j(\omega)$. Also, it is clearly seen from the graph below that JONSWAP wave spectrum $S_j(\omega)$ has more energy than Pierson-Moskowitz $S_{PM}(\omega)$ wave spectrum at the natural frequency (i.e. ω_0 = 0.64rad/s) in heave of the platform.

REFERENCE

[1] REN21, "Renewables 2016: Global Status Report; REN21." Secretariat Paris, 2016.

[2] M. N. Kaya, F. Kose, D. Ingham, L. Ma, and M. Pourkashanian, "Aerodynamic performance of a horizontal axis wind turbine with forward and backward swept blades," *J. Wind Eng. Ind. Aerodyn.*, vol. 176, pp. 166–173, 2018, doi: https://doi.org/10.1016/j.jweia.2018.03.023.

[3] P. Larin, M. Paraschivoiu, and C. Aygun, "CFD based synergistic analysis of wind turbines for roof mounted integration," *J. Wind Eng. Ind. Aerodyn.*, vol. 156, pp. 1–13, 2016.

[4] M. Moshfeghi, S. Shams, and N. Hur, "Aerodynamic performance enhancement analysis of horizontal axis wind turbines using a passive flow control method via split blade," *J. Wind Eng. Ind. Aerodyn.*, vol. 167, pp. 148–159, 2017.

[5] M. Purusothaman, T. N. Valarmathi, and S. P. Reddy, "Selection of Twist and Chord Distribution of Horizontal Axis Wind Turbine in Low Wind Conditions," *IOP Conf. Ser. Mater. Sci. Eng.*, vol. 149, p. 012203, 2016, doi: 10.1088/1757-899X/149/1/012203.

[6] A. Ahlström, "Aerolastic simulation of wind turbine dynamics." KTH, 2005.

[7] M. R. Ahmed, "Blade sections for wind turbine and tidal current turbine applications–current status and future challenges," *Int. J. Energy Res.*, vol. 36, no. 7, pp. 829–844, 2012.

[8] E. A. Bamidele, "Adsorption of Arsenic on Lanthanum and Cerium nanoparticles adsorbents during hydrometallurgical extraction of Copper."

[9] D. Schlipf *et al.*, "Testing of frozen turbulence hypothesis for wind turbine applications with a scanning lidar system," 2010.

[10] B. Emmanuel, J. A. Ajayi, and E. Makhatha, "Investigation of Copper Recovery rate from Copper Oxide Ore Occurring as Coarse Grains Locked in a Porphyritic Fine Grain Alumina and Silica," *Energy Procedia*, vol. 157, pp. 972–976, 2019, doi: https://doi.org/10.1016/j.egypro.2018.11.264.

[11] S. Liu and I. Janajreh, "Development and application of an improved blade element momentum method model on horizontal axis wind turbines," *Int. J. Energy Environ. Eng.*, vol. 3, no. 1, p. 30, 2012.

[12] B. Emmanuel, E. Makhatha, and W. Nheta, "A Review of Lanthanum Nanoparticles Impregnated Compound Arsenic Fixation Behaviour in Copper Aqueous Solution," *Energy Procedia*, vol. 157, pp. 966–971, 2019, doi: https://doi.org/10.1016/j.egypro.2018.11.263.

[13] E. Bamidele, X. Chen, J. Durm, C. Park, J. MacLennan, and N. Clark, "Behavior of Superparamagnetic Microbeads in Smectic Films," *Bull. Am. Phys. Soc.*, 2020.

[14] F. J. Xu, F. G. Yuan, J. Z. Hu, and Y. P. Qiu, "Miniature horizontal axis wind turbine system for multipurpose application," *Energy*, vol. 75, pp. 216–224, 2014.

[15] A. O. Ijaola, P. K. Farayibi, and E. Asmatulu, "Superhydrophobic coatings for steel pipeline protection in oil and gas industries: a comprehensive review," *J. Nat. Gas Sci. Eng.*, vol. 83, p. 103544, 2020, doi: 10.1016/j.jngse.2020.103544.

[16] B. Emmanuel, A. J. Ade, and E. Makhatha, "Mineralogical Study of Pingel-Bauchi Malachite Ore," in *ASETH-18*, 2018, vol. 10, no. Advances in Science, Engineering, Technology & Healthcare (ASETH-18), p. 10, doi: https://doi.org/10.17758/EARES4.EAP1118203.

[17] A. O. Ijaola, R. Asmatulu, and K. Arifa, "Metal-graphene nano-composites with enhanced mechanical properties," in *Behavior and Mechanics of Multifunctional Materials IX*, 2020, vol. 11377, p. 113771E.

[18] J. IRENA, "Renewable energy technologies: cost analysis series. Concentrating Solar Power," *Compr. Renew. Energy*, vol. 3, no. 2, 2012.

[19] T. Nishino, *BEM models for HAWT ' s Further reading*. CRANFIELD, 2017.

[20] G. Ingram, "Wind Turbine Blade Analysis using the Blade Element Momentum Method. Version 1.1," *October*, no. c, pp. 1–21, 2011.

[21] D. N. Veritas, "Environmental conditions and environmental loads," *Dnv*, no. October, pp. 9–123, 2010, doi: 10.1109/INTLEC.1993.388591.

[22] M. Collu, *Ocean waves : deterministic and probabilistic modelling approaches (L3-1)*. CRANFIELD, 2017.

[23] R. Shirzadeh, W. Weijtjens, P. Guillaume, and C. Devriendt, "The dynamics of an offshore wind turbine in parked conditions: a comparison between simulations and measurements," *Wind Energy*, vol. 18, no. 10, pp. 1685–1702, 2015.

[24] R. Shirzadeh, C. Devriendt, M. A. Bidakhvidi, and P. Guillaume, "Experimental and computational damping estimation of an offshore wind turbine on a monopile foundation," *J. Wind Eng. Ind. Aerodyn.*, vol. 120, pp. 96–106, 2013.

[25] M. Collu, *Fluid loading on offshore structures*. CRANFIELD, 2017.

[26] J. Wienke and H. Oumeraci, "Breaking wave impact force on a vertical and inclined slender pile—theoretical and large-scale model investigations," *Coast. Eng.*, vol. 52, no. 5, pp. 435–462, 2005.

[27] J. F. Wilson, *Dynamics of offshore structures*. John Wiley & Sons, 2003.

[28] A. Ijaola, K. Arifa, E. Jurak, H. Misak, and R. Asmatulu, "Effects of acid treatments on physical properties of CNT wires for wiring applications," in *Nano-, Bio-, Info-Tech Sensors, and 3D Systems IV*, 2020, vol. 11378, p. 113780C.

[29] P. Kaplan, "Wave impact forces on offshore structures: re-examination and new interpretations," 1992.

[30] O. Olaniran, O. Uwaifo, E. Bamidele, and B. Olaniran, "An investigation of the mechanical properties of organic silica, bamboo leaf ash and rice husk reinforced aluminium hybrid composite," *Mater. Sci. Eng. Int. J.*, vol. 3, no. 4, Jul. 2019, doi: 10.15406/mseij.2019.03.00103.

[31] M. Patel, *Dynamics of offshore structures*, vol. 7, no. 3. 1985.

[32] A. O. Ijaola *et al.*, "Wettability Transition for Laser Textured Surfaces: A Comprehensive Review," *Surfaces and Interfaces*, p. 100802, 2020, doi: https://doi.org/10.1016/j.surfin.2020.100802.

[33] T. Diveux, P. Sebastian, D. Bernard, J. R. Puiggali, and J. Y. Grandidier, "Horizontal axis wind turbine systems: optimization using genetic algorithms," *Wind Energy An Int. J. Prog. Appl. Wind Power Convers. Technol.*, vol. 4, no. 4, pp. 151–171, 2001.

[34] S. Naderi, S. Parvanehmasiha, and F. Torabi, "Modeling of horizontal axis wind turbine wakes in Horns Rev offshore wind farm using an improved actuator disc model coupled with computational fluid dynamic," *Energy Convers. Manag.*, vol. 171, pp. 953–968, 2018.

[35] M. Islam, M. R. Amin, D. S.-K. Ting, and A. Fartaj, "Aerodynamic factors affecting performance of straight-bladed vertical axis wind turbines," in *ASME international mechanical engineering congress and exposition*, 2007, vol. 43009, pp. 331–341.